# New Methods of Induction Motor Torque Regulation

A. B. PLUNKETT, MEMBER, IEEE, AND THOMAS A. LIPO, SENIOR MEMBER, IEEE

*Abstract*—**Two methods of induction motor torque regulation are described utilizing speed and current feedback into the frequency and amplitude channels of a pulsewidth modulated inverter. Transfer characteristics illustrating the steady-state behavior of the two configurations are presented. Transient characteristics are discussed in detail by examining the linearized system transfer functions. An analytical approach to design of a closed loop controller for a practical application is outlined. Experimental results are presented showing correlation with predicted results.**

## INTRODUCTION[1]

THE DEVELOPMENT of static adjustable frequency power converters has opened up new fields of application for ac machines. These new applications have, in turn, resulted in a need for new approaches to the control of ac motors. Probably the most important type of motor control is the torque controller, since it also forms the inner loop for many types of speed and position controllers as well. An application having particularly stringent performance requirements is a traction drive in which rapid and precise torque regulation is desirable for smooth acceleration. Inherent advantages of the ac traction system include: 1) absence of starting resistors; 2) possibility of power regeneration; 3) few mechanical switches; 4) low motor maintenance; and 5) high motor efficiency.

In the case of dc machines, sensing of armature and field currents will yield a fairly accurate measure of the flux level in the machine, and hence, the developed torque. However, the flux and torque of an induction motor are not as easily measured, particularly when the voltage supplied to the terminals of the machine is not sinusoidal.

In this paper, two general methods for accurate torque regulation of an induction motor drive are presented. The two methods both involve regulation of the flux level of the induction motor by control of slip frequency and stator current. Two different functions of stator current are investigated consisting of current magnitude and the real component of current with respect to voltage behind the stator $IR$ drop. Transfer characteristics illustrating steady-state behavior are discussed. The linearized system transfer functions for various types of feedback are examined and a feedback control system devised to satisfy performance constraints. Experimental data are presented to demonstrate the torque accuracy to be expected with this type of regulator.

Paper TOD-75-44, approved by the Static Power Converter Committee of the IEEE Industry Applications Society for presentation at the 1974 Ninth Annual Meeting of the IEEE Industry Applications Society, Pittsburgh, PA, Oct. 7–10. Manuscript released for publication May 5, 1975.

A. B. Plunkett is with the General Electric Company, Erie, PA 16501.

T. A. Lipo is with the General Electric Company, Schenectady, NY.

[1] Nomenclature explained at the end of this paper.

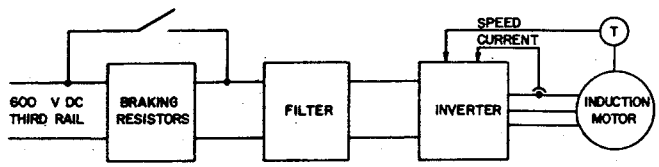


Fig. 1. Basic ac transit car propulsion system.

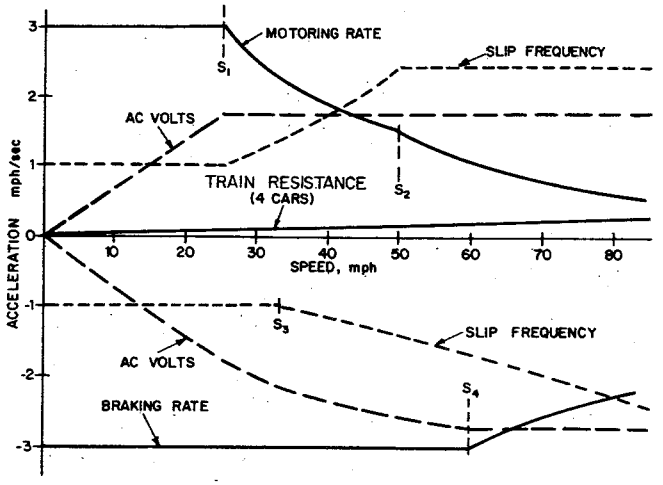


Fig. 2. Transit car performance curves.

## SYSTEM CHARACTERISTICS

Although torque regulation is a desirable feature for numerous applications, the drive considered in this paper is to be applied to a transit application. Hence, a brief description of the system configuration and special requirements will aid in understanding the control system operation. A simplified block diagram of an overall dc/ac transit car propulsion system is shown in Fig. 1. The propulsion drive is designed to operate from a conventional 600 V dc third rail supply. Raw dc voltage is fed from the rail to a filter which serves to supply reactive power to the motor and to isolate the inverter from fast line transients. Power is then converted from dc to adjustable frequency, adjustable amplitude ac by means of a pulsewidth modulated voltage inverter. The inverter is sinusoidally pulsewidth modulated at low frequencies so as to shape the ac voltage wave. The conventional dc traction motor is replaced with an ac induction motor with associated controls. Since the motors are to brake electrically both when connected (regeneration) and when isolated from the supply (dynamic braking), a resistor and contactor arrangement is used for braking.

The general form of a typical car performance curve is shown in Fig. 2. This figure shows acceleration, motor voltage, slip frequency, and drain resistance as a function of car speed. The motoring curve consists of three major

portions: 1) a constant tractive effort section to speed $S_1$ necessitating constant torque from the motor; 2) a constant horsepower section from $S_1$ to $S_2$; and 3) a motoring portion at reduced flux from $S_2$ to the maximum speed. The torque limited (constant acceleration) section results from considerations of passenger comfort and wheel adhesion. The constant horsepower section corresponds to the field weakening mode of operation of a dc motor and arises from two considerations: a limitation exists on the capability of the distribution system to supply power to the car, and the power is limited on the size of the components in the car propulsion equipment. The section of the motor curve from $S_2$ to maximum speed corresponds to operation of the motor at breakdown torque with the maximum available voltage from the inverter. Thus the tractive effort is inversely proportional to speed squared. In general, this section of the curve corresponds to the torque characteristic of a series dc motor, although the curve for a dc motor falls somewhat below this curve due to the main filed magnetic circuit saturation.

The braking curve has two sections. The first section is a constant deceleration rate in the speed range from zero to $S_4$. The second is the constant power taper, which again is the most practical characteristic for a power limited propulsion system and corresponds to available wheel-rail adhesion limits. The train resistance curve corresponds to a four-car train. The train resistance subtracts from the motoring tractive effort to give an acceleration somewhat less than indicated on the curve and adds to the braking rate so that the braking deceleration is greater than that due to the electric or friction brake alone. It is clear that the shape of the torque-speed curve is partly dictated by motor characteristics and partly by power distribution system limitations, which in turn cause additional restrictions on the motor design. Smooth torque control is necessitated for passenger comfort. Accurate torque regulation is required to allow predictable performance for automatic train control.

From Fig. 2 it is apparent that the motor control can be divided into three modes of operation: mode I for speeds of zero to $S_1$ in which slip frequency is held constant with the motor terminal voltage increasing linearly with speed; mode II between speeds $S_1$ and $S_2$ in which voltage is held constant with slip frequency increasing with speed; mode III for speed $S_2$ to maximum speed for which both voltage and slip frequency are constant. Analogous modes also exist in braking operation with the transition between modes I and II at speed $S_4$. By proper sizing of braking resistors, mode III can be avoided in braking.

In order to operate over the entire permissible operating range specified by Fig. 2, it is desirable to devise a torque and power regulator which will transfer smoothly from mode I when both voltage and slip frequency are controlled, to mode II during which only voltage is controlled, to mode III when both voltage and frequency are to be held constant. Although Fig. 2 indicates only maximum motor and braking performance, steady-state operation at any value between these limits must be achievable.

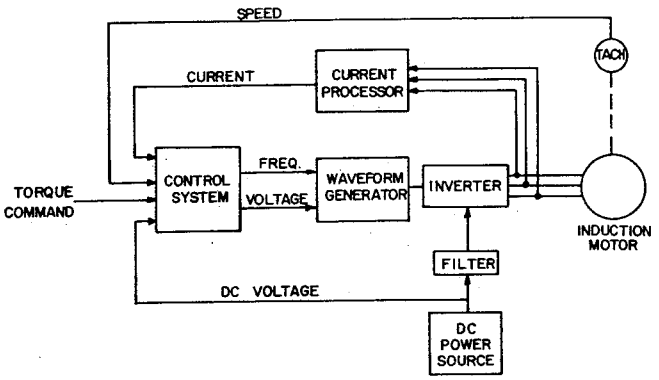


Fig. 3. Basic control system.

Fig. 3 shows a simplified block diagram illustrating the essential features of a control scheme capable of meeting these requirements. Rotor speed and line current are monitored and fed back to the control input. The two control channels are the frequency input to the inverter which adjusts the motor slip frequency to control current and the voltage control which adjusts the amplitude of the motor voltage to force the slip frequency to the correct value.

A major design problem in this type of system is the selection of the type of current processing for use in the current feedback element. The requirements for the current processing element are critical since the level of motor flux will be regulated using this signal. In general, selection of proper feedback quantities involves two considerations: 1) steady-state accuracy or ability of the controlled variables to regulate the required output quantity, that is, shaft torque, and 2) transient response or ability of the controlled variables to move rapidly from one steady-state operating point to another. In the following sections the steady-state and transient behavior of three possible methods of current feedback will be discussed: 1) average rectified current or current magnitude; 2) average component of stator current in phase with the applied voltage (real current); and 3) average component of stator current in phase with the voltage inside the stator $IR$ drop (modified real current).

## STEADY-STATE TRANSFER CHARACTERISTICS

### *Current Magnitude Feedback*

Probably the simplest scheme for regulating torque from the conceptual point of view is the use of current magnitude and slip frequency. The principle behind this technique is readily deduced from the basic per-phase motor equivalent circuit shown in Fig. 4. Consider operation with a sinusoidal current having amplitude $i_1$, corresponding to balanced three-phase steady-state operation. It is clear that reactances $\omega_e L_m$, $\omega_e L_{lr}$, and $\omega L_{ls}$ are proportional to the inverter frequency $\omega_e$. However, since $r_r/S = \omega_e r_r/(\omega_e - \omega_r)$ the equivalent rotor resistance is also proportional to frequency provided that the slip angular frequency $\omega_{sl} = \omega_e - \omega_r$ is held constant. Since $\omega_e L_m$,

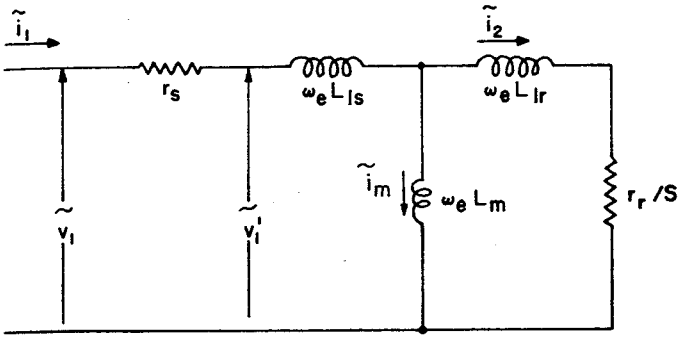


Fig. 4. Per-phase induction motor equivalent circuit.

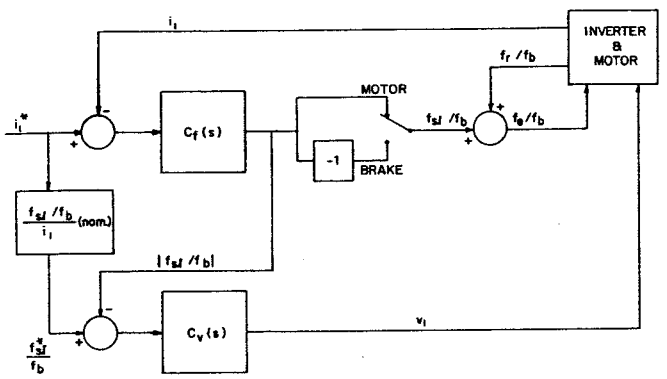


Fig. 5. Torque control system using current magnitude and speed feedback.

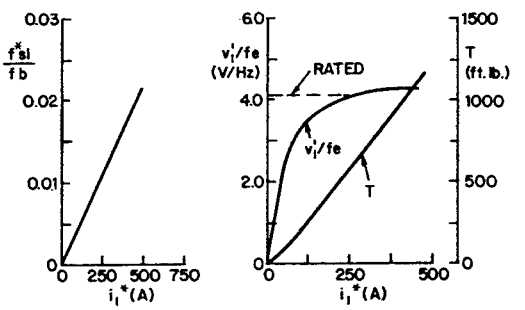


Fig. 6. Transfer characteristics, linear $f_{sl}^* - i_1^*$ relation.

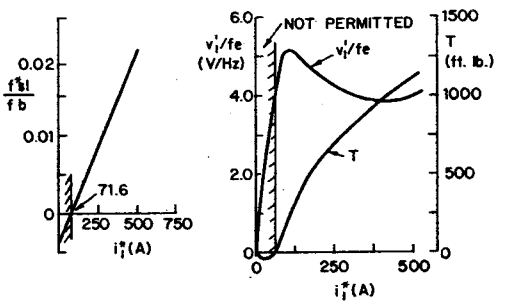


Fig. 7. Transfer characteristics, offset $f_{sl}^* - i_1^*$ relation; $i_1^*$ less than 71.6 A not permitted.

$\omega_e L_{lr}$ and $r_r/S$ are then proportional to frequency, it is clear that phasors $\tilde{i}_2$ and $\tilde{i}_m$ will be fixed if slip frequency and $\tilde{i}_1$ are constant. Because torque is proportional to $(i_2^2)r_r/S$, it follows that torque will also be constant. In addition, it is clear that $i_1^2 r_s$ and $i_2^2 r_r$ or stator and rotor power losses are also fixed under these constraints. Output power, on the other hand, increases linearly with rotor speed.

Fig. 5 shows a simplified control block diagram using current magnitude and speed feedback. Current $i_1^*$ and $f_{sl}^*/f_b$ denote the commanded values of current and slip frequency. Compensators $C_f(s)$ and $C_v(s)$ can be regarded tentatively as integrators or high gains which zero the error at the two summing points during steady-state operation. Quantities $f_e$, $f_r$, $f_{sl}$, and $f_b$ denote the stator (inverter) frequency, equivalent rotor speed in hertz, slip frequency, and base frequency, respectively. Although not required, it has been found convenient to express the line, rotor, and slip frequency as a per unit of base frequency as noted on the figure. A proportional gain $(f_{sl}/f_b)/i_1(\text{nom.})$ is set such that when the commanded current $i_1^*$ is equal to nominal current at the upper summing point; then nominal slip frequency is demanded at the lower summing point. Since, in the steady-state, current magnitude and slip frequency are maintained constant by the above argument, torque will also be held constant independent of rotor speed. It should be noted that changes in stator resistance and stator leakage reactance have no effect on the torque set point. In addition, variations in magnetizing reactance have only minimal effect on the resulting output torque, since at normal levels of current the magnetizing current is relatively small.

Fig. 6 shows the resulting steady-state transfer characteristic between torque and the current magnitude input command signal $i_1^*$. Also plotted on Fig. 6 are the volts per hertz corresponding to the voltage across stator flux $v_1'$ as noted on Fig. 4. The proportional gain of Fig. 5 has been set for nominal operation at 750 ft·lb. For this case, the slip frequency $f_{sl}^*/f_b$ is 0.013 when $i_1^*$ is 291.6 A. It should be noted that the transfer characteristics are independent of stator frequency and hence are valid for any speed in mode I. In general, only positive values of $i_1$ are admissible. Braking is achieved by demanding the same value of current magnitude with the switch of Fig. 5 in the brake position. This results in an equal value of $v_1'/f_e$ and the same (but negative) value of torque.

It can be seen that the torque-current characteristic is nearly linear when $i_1^*$ is greater than 75 A (magnetizing current). However, excitation is correct only at the set point of 750 ft·lb, and a no-load operating condition can only be achieved by reducing the volts per hertz and hence, motor flux to zero. This condition is clearly unsuitable since zero voltage is achieved by switching the inverter at a maximum rate resulting in high system losses at no-load.

An improved characteristic is plotted in Fig. 7. In this case, the linear relationship between commanded current and slip frequency has been altered so that the slip frequency is zero when $i_1^*$ equals magnetizing current. Values of $i_1^*$ less than magnetizing current are not permitted. It can be noted that the torque-current command characteristic is less linear than that of Fig. 5 although not unduly so. A more serious problem is revealed from

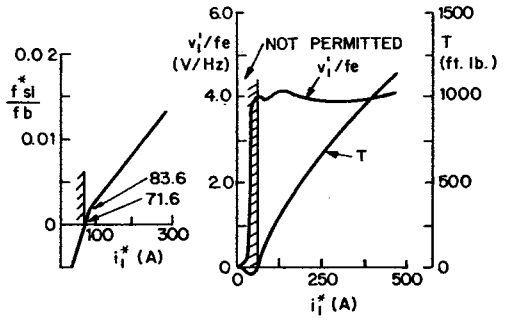


Fig. 8. Transfer characteristics, breakpoint in $f_{sl}^* - i_1^*$ relation; $i_1^*$ less than 71.6 A not permitted.

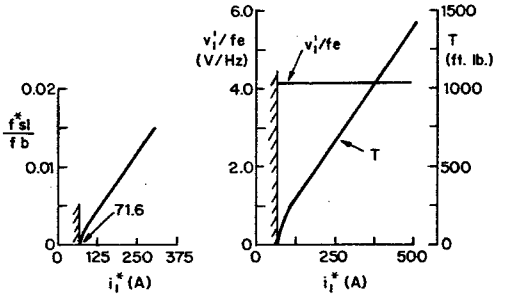


Fig. 9. Transfer characteristics, nonlinear $f_{sl}^* - i_1^*$ relation; $i_1^*$ less than 71.6 A not permitted.

the volts per hertz–current plot which indicates that the motor will run saturated at light loads.

In Fig. 8 the functional relationship between current and slip frequency has been changed to a nonlinear characteristic in an effort to reduce motor voltage at light loads. A single break has been introduced at 83.3 A. It is seen that the increase in $v_1'/f_e$ at light loads has been reduced to an acceptable value. If necessary, additional breaks in the characteristic could be introduced to flatten the curve still further. The ideal characteristic of $f_{sl}^*/f_b$ versus $i_1^*$ required to achieve this effect is given in the left side of Fig. 9. This is ideal because the corresponding volts per hertz versus current curves are horizontal lines; thus a varying load does not affect the flux level.

*Real Current Feedback*

In its simplest form the real component $i_{1,\mathrm{Re}}$ of terminal current $i_1$ relative to the terminal voltage $v_1$ can be maintained constant. Motor slip frequency is adjusted in proportion to the real component of current. Since input power is $v_1 i_{1,\mathrm{Re}}$ frequency in mode I, the input power increases linearly with frequency, implying a constant output torque independent of motor speed. However, the result is only approximate since the power loss in the motor modifies the results.

The system block diagram for real current control shown in Fig. 10 is similar to Fig. 4 except that $i_1^*$ is replaced by $i_{1,\mathrm{Re}}^*$, and the proportional block relating slip frequency to current is altered appropriately. The sign change in the frequency loop for braking is not required but must instead be placed in the voltage loop.

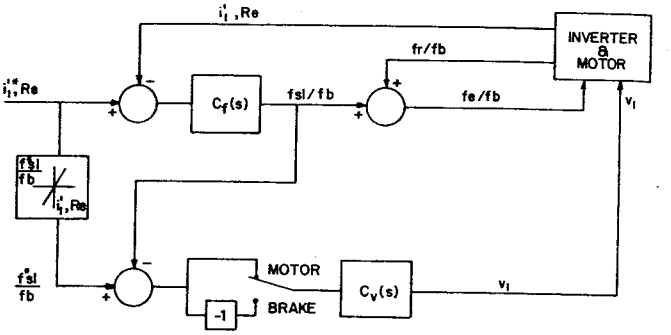


Fig. 10. Torque control system using real component of current and speed feedback.

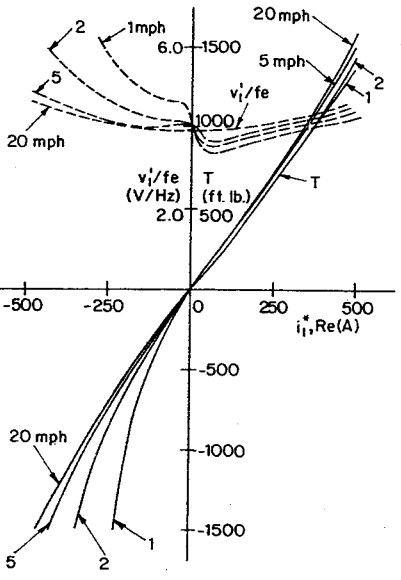


Fig. 11. Transfer characteristics using linear $f_{sl}^* - i_{1,\mathrm{Re}}^*$ relation; $f_{sl}^*/f_b = 4.9 \cdot 10^{-4} i_{1,\mathrm{Re}}^*$.

Fig. 11 shows the transfer characteristic between commanded current $i_{1,\mathrm{Re}}^*$ and the resulting torque and volts per hertz $v_1'/f_e$ assuming a linear relationship between current command and slip command. Operation at speeds of 20, 5, 2, and 1 mi/h are shown. For motoring operation (positive $i_{1,\mathrm{Re}}^*$), it is apparent that the control scheme will yield adequate performance. Although the output torque is not independent of frequency, the effect of frequency changes is small. Similarly, the line current magnitude $i_1$ and volts per hertz $v_1'/f_e$ are relatively insensitive to frequency changes indicating satisfactory performance over the entire speed range for any motoring load. Severe problems are, however, apparent for braking. For a fixed value of $i_{1,\mathrm{Re}}$ and $f_{sl}/f_b$, the torque magnitude increases substantially as frequency is reduced. A more serious defect is evident from the plot of $v_1'/f_e$. It is seen that during low speed braking the volts per hertz across the stator flux linkage rises rapidly and motor saturation will occur. Also, it can be shown that although the real component of current is under control, the magnitude of current rises rapidly with braking effort at low speeds putting an overload on the inverter.

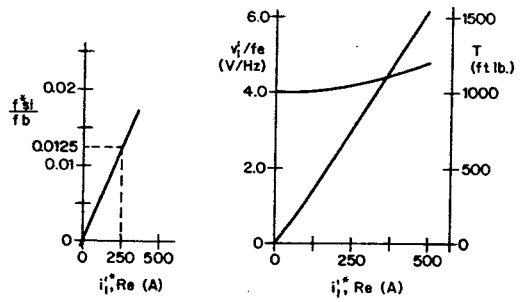


Fig. 12. Transfer characteristics using linear $f_{sl}^* - i_{1,Re}'^*$ relation.

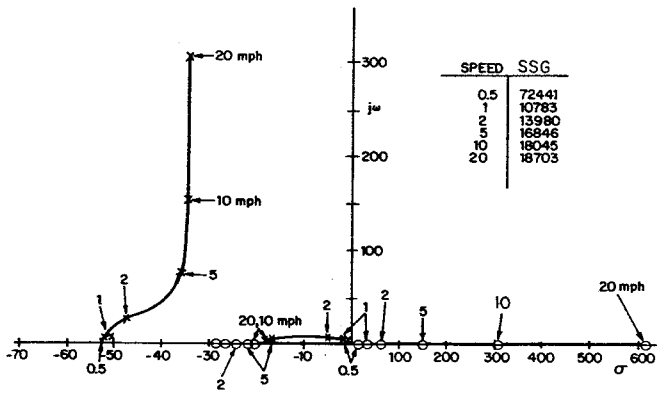


Fig. 13. Poles and zeros of TF $\Delta i_1/(\Delta f_e/f_b)$, motoring at 750 ft·lb, $\Delta_{v1} = 0$. Note change in abcissa scale.

*Control Using Modified Real Current*

A technique which eliminates many of the problems associated with a real current component is to regulate the real component of current relative to the voltage across stator flux linkage $v_1'$ rather than the terminal voltage $v_1$. The corresponding current magnitude is denoted by $i_1'$ and the real component $i_{1,Re}'$. Fig. 12 shows the effect on torque and voltage when the slip frequency command $f_{sl}^*/f_b$ is adjusted linearly with $i_{1,Re}'^*$. Chosen as nominal values of $i_{1,Re}'$ and $f_{sl}/f_b$ are those values which result in rated torque and rated motor air-gap flux. Again, 750 ft·lb was chosen as the nominal value of torque. Torque and stator flux linkage (or $v_1'/f_e$) are now maintained constant independent of speed. The volts per hertz rises with increased loads, but not severely. If necessary, the rising characteristic can be eliminated by using a nonlinear relationship between $f_{sl}/f_b$ and $i_{1,Re}'$.

## OPEN-LOOP TRANSIENT BEHAVIOR

The analysis of the previous section indicates that good steady-state torque regulation can be achieved by regulating slip frequency together with current magnitude or the component of current associated with air-gap power. However, dynamic performance of the system has not been considered. Compensators must be designed so that the commanded operating point is, in fact, achieved. In order to evaluate the transient performance of these control schemes, the system equations can be linearized so as to describe system behavior for small changes around an operating point [1]–[3]. Fig. 13 shows the migration of the poles and zeros for the open-loop transfer function corresponding to a change in magnitude of current output with a change in frequency as input $\Delta i_1(\Delta f_e/f_b)$, wherein the steady-state motor speed is used as a parameter. The steady-state slip frequency and current magnitude were fixed so as to produce maximum motoring effort (750 ft·lb). Since the effective inertia of the transit car is approximately 50 times nominal rotor inertia, the rotor speed is assumed constant throughout the analysis. Also, the effects of the finite source impedance (filter) on motor behavior are not considered initially.

When speed is constant, the motor is characterized by two pairs of poles at each load point. The pair of high-frequency poles (at 300 rad/s for 20 mi/h) are associated with stator current dc offsets. The real part of the roots corresponds approximately to the reciprocal of the stator transient time constant. The frequency component of these roots is nearly equal to the applied angular frequency. The low-frequency pair of poles is associated with the steady-state operating point. The real part is given approximately by the reciprocal of the rotor transient time constant. The frequency component is related (but not proportional) to the slip angular frequency. While the low-frequency poles are highly damped, it is observed that the high-frequency poles will result in an oscillatory response.

It can be noted that the low-frequency "rotor" poles are relatively independent of applied frequency while the frequency component of the high-frequency "stator" poles are nearly equal to line frequency. The real component of the rotor poles decreases rapidly between 5 and 2 mi/h (approximately 13 and 3 Hz). Minimum damping is realized at low speed.

The motion of the poles and zeros presents a difficult problem in the design of an effective feedback compensator. Reference to Fig. 13 indicates that one of the two low-frequency poles is effectively cancelled by the left half-plane (LHP) zero at high frequencies and the right half-plane (RHP) zero at low frequencies resulting in a 20 dB/dec break and 90° phase shift in the frequency response. This break can be effectively cancelled by a lead network which essentially inserts an additional zero positioned at this frequency in the composite transfer function. The high-frequency poles introduce an additional 40 dB/dec break and 180° phase shift at a point fixed essentially by the line frequency. An upward break is contributed by the RHP zero at a somewhat higher frequency. It is apparent that the low damping of the high-frequency poles results in a peaking in the Bode magnitude plot at the line frequency. Compensation of these poles presents a much more difficult problem since the compensator zeros must be expected to "track" these poles as frequency varies. Alternatively, the compensator zero can be set for the worst case condition (low-frequency operation) which will result in a sluggish system with a low crossover frequency. In addition to the motion of the poles and zeros, it can be noted from Fig. 13 that the steady-state gain (SSG) varies widely as speed (line frequency) is

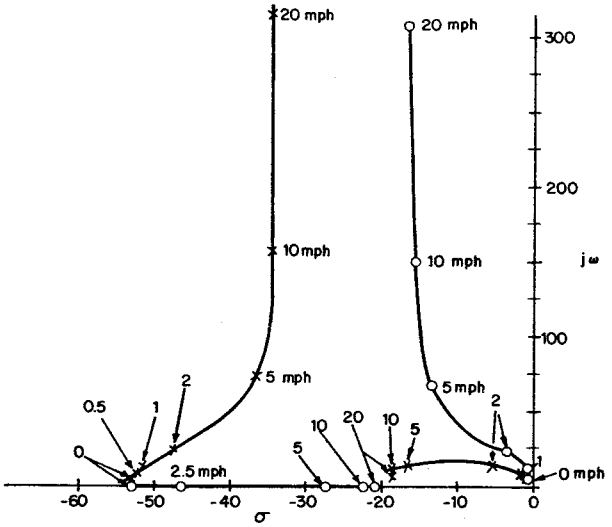


Fig. 14. Poles and zeros of TF $\Delta i_1'/(\Delta f_e/f_b)$, motoring at 750 ft·lb constant V/Hz ($\Delta_{v1} + 0$).

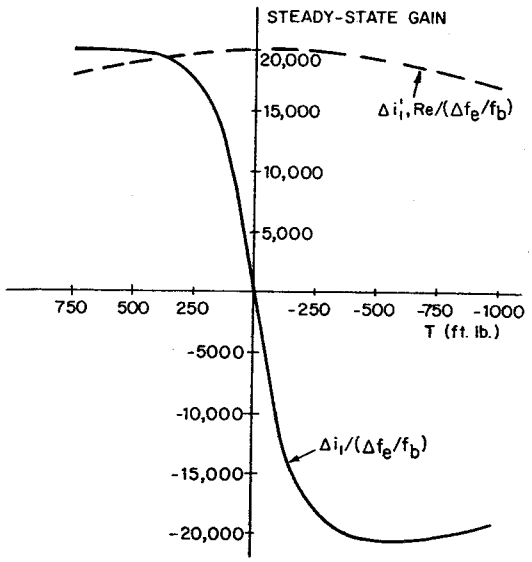


Fig. 15. Steady-state gain for varying load at 20 mi/h.

reduced implying the need of a compensator gain proportional to speed.

The difficulty associated with compensating the high-frequency poles can be eliminated by introducing a multiplier in the voltage channel such that

$$v_1 = \frac{f_e}{f_b} V_1. \tag{1}$$

It can be noted that the new variable $V_1$ corresponds to a volts per hertz signal. Hence, $V_1$ is nominally a constant and varies with speed or load only to account for the stator $IR$ drop. The transfer function corresponding to $\Delta i_1/(\Delta f_e/f_b)$ (magnitude of current feedback) incorporating the constraint of (1) is given in Fig. 14. With this type of control, a significant change is noted in the transfer function. It is seen from Fig. 14 that a pair of conjugate zeros are now located near the high-frequency poles. These zeros follow the corresponding poles as frequency is reduced, approximately cancelling their effect in the overall transfer function. This pole-zero cancellation is clearly a useful property and can be utilized in the design of a proper feedback stabilization network except at very low speeds. It can be seen that the pair of conjugate zeros tracking the high-frequency and the zero near the low-frequency poles interchange roles between 5 and 2 mi/h so that the high-frequency zero begins to track the low-frequency rotor poles below 2 mi/h. Hence, for motoring the region 2–5 mi/h can be considered the area of most concern in the design of the feedback compensator.

A significant advantage in real current feedback can be noted in Fig. 15 by comparing operating points for various load conditions to similar points employing current magnitude feedback. Whereas the SSG of $\Delta i_1/(\Delta f_e/f_b)$ changes sign, the SSG of $\Delta i_{1,\mathrm{Re}}'/(\Delta f_e/f_b)$ is relatively constant and does not reverse sign between motoring and braking. Hence, current magnitude control is ineffective at no-load. However, use of real component of current will result in good inherent damping for all load conditions. The effect

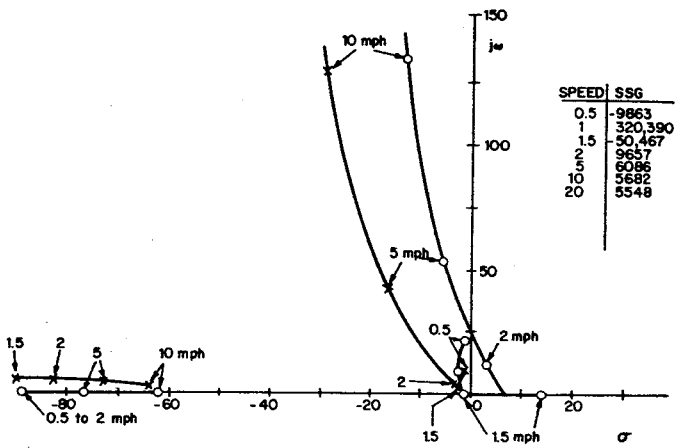


Fig. 16. Poles and zeros of TF $\Delta i_{1,\mathrm{Re}}/(\Delta f_e/f_b)$, braking at −910 ft·lb, constant V/Hz ($\Delta V_1 = 0$).

of the operating speed on the transfer function $\Delta i_{1,\mathrm{Re}}'/(\Delta f_e/f_b)$ during motoring is similar to $\Delta i_1/(\Delta f_e/f_b)$. Coupling the frequency to the voltage channel by means of (1) again improves system characteristics. A pair of conjugate poles effectively cancels the stator poles resulting in a well-behaved equivalent first-order transfer function with a single break of 20 dB/dec at approximately 20 rad/s. Poles and zeros of this transfer function as a function of speed for maximum braking effort are summarized in Fig. 16.

At 5 mi/h, the real part of the complex zeros tracking the stator poles begins to change rapidly and at 3.2 mi/h appear in the RHP. The zeros remain in the RHP for a short time and then return to the LHP. After returning to the LHP, the SSG increases markedly before returning to the nominal value of 1500 at zero speed.

## COMPENSATOR DESIGN

The behavior of the system poles and zeros clearly presents a difficult problem in compensator design. The

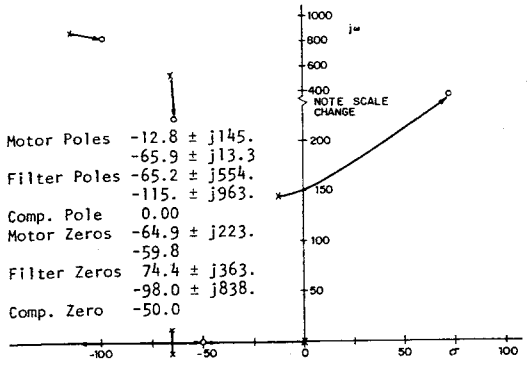


Fig. 17. Root locus of closed-loop transfer function $i_{1,\mathrm{Re}}/(\Delta f_e/f_b)$, motoring at 750 ft·lb, 20 mi/h. Effect of filter included.

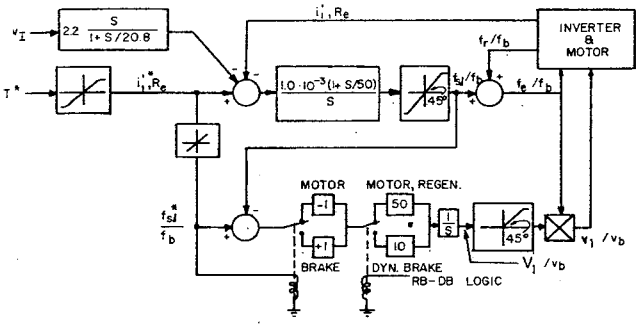


Fig. 18. Final torque control system.

open loop system, of course, is always stable since the system poles remain in the LHP. When all system zeros are also in the LHP, compensation is not difficult since the excess of poles over zeros is one. During motoring and high-speed regenerative braking, all zeros appear in the LHP. However, a pair of zeros corresponding to the stator circuit migrates to the right as speed decreases and enters the RHP at approximately 3 mi/h when braking at the maximum rate. Hence, unless special precautions are taken, braking torque will not be regulated below this speed.

Since a high-speed motoring situation can be considered more important than low speed braking, the case of motoring at 20 mi/h, 750 ft·lb was selected as the design point. A proportional plus integral compensator was chosen. Fig. 17 shows a sample root locus plot for the optimum compensator at this nominal load condition. In this case a complete analysis was undertaken so that in Fig. 17 the effect of the filter poles as well as the motor poles have been accounted for [2]. In Fig. 18 the loop from real current to frequency has been closed through the chosen compensator $(C_f)$. The poles and zeros of the transfer function $(\Delta V_1/v_b)/(\Delta f_{sl}/f_b)$ required for design of the compensator in the voltage channel are shown for two representative operating conditions. It can be noted that for the case 750 ft·lb and 20 mi/h, two pairs of zeros exist in the RHP. The most significant zeros are the stator zeros which limit the crossover frequency at this operating point to less than 50 rad/s (approximately). As load decreases, these zeros move to the left and the SSG

TABLE I

POLES AND ZEROS OF TF $(\Delta f_{sl}/f_b)/(\Delta V_1/v_b)$; $C_f = 1.0\cdot10^{-3}$ $(1 + s/50)/s$ IN FREQUENCY CHANNEL; EFFECT OF DC FILTER AND REGEN; BRAKING RESISTOR INCLUDED

| | | | | |
|---|---|---|---|---|
| 750 ft. lb. | SSG | -0.0548 | | |
| 20 mph | Poles | -5.00 | | (comp.) |
| | | -67.2 | ± j13.2 | (rotor) |
| | | -10.5 | ± j145. | (stator) |
| | | -67.1 | ± j552. | (filter) |
| | | -115. | ± j863. | (filter) |
| | Zeros | -50.6 | | (comp.) |
| | | -110. | | (rotor) |
| | | 8.67 | ± j46.9 | (stator) |
| | | 19.0 | ± j255. | (filter) |
| | | -100. | ± j838. | (filter) |
| -750 ft. lb. | SSG | 0.095 | | |
| 20 mph | Poles | -11.3 | | (c) |
| | | -33.2 | | (r) |
| | | -104. | | (r) |
| | | -147. | ± j79.3 | (s) |
| | | -100. | ± j417. | (f) |
| | | -178. | ± j796. | (f) |
| | Zeros | -51.4 | | (c) |
| | | 39.5 | | (r) |
| | | -65.7 | ± j34.6 | (s) |
| | | -231. | ± j196. | (f) |
| | | -189. | ± j784. | (f) |

TABLE II

DOMINANT POLES OF CLOSED LOOP TF $\Delta i_{1,\mathrm{Re}}'/\Delta i_{1,\mathrm{Re}}'^*$ FOR NEAR OPTIMUM GAIN; $C_f = 1.0\cdot10^{-3}$ $(1 + s/50)/s$ IN FREQUENCY CHANNEL; $C_v = K_v/s$ IN VOLTAGE CHANNEL

| | |
|---|---|
| 20 mph, 750 ft.lb. | -2.42 ± j2.78 |
| Motoring, $K_v$=-50 | -10.5 ± j146. |
| 2 mph, 750 ft.lb. | -2.45 ± j2.65 |
| Motoring, $K_v$=-50 | -2.99 ± j34.2 |
| 20 mph, -910 ft.lb. | -5.23 ± j0.37 |
| Regen Braking, $K_v$=20 | -31.2 |
| 2 mph, -345 ft.lb. | -0.60 |
| Regen Braking, $K_v$=20 | -0.80 ± j1.2 |
| 20 mph, -910 ft.lb. | -1.63 |
| Dynamic Braking, $K_v$=10 | -2.0 ± j12.4 |
| 5 mph, -910 ft.lb. | -0.59 |
| Dynamic Braking, $K_v$=7 | -0.58 ± j9.55 |

decreases. During braking, the stator zeros are in the LHP, again limiting crossover frequency, this time to values less than 40 rad/s (at −750 ft·lb). Since the poles of the system vary widely with load and speed when the loop is closed between $\Delta i_{1,\mathrm{Re}}'$ and $\Delta f_e/f_b$, fixed compensator techniques for the second (voltage) control loop are difficult to apply. (See Table I.)

Table II considers the use of pure integration $C_v = K_v/s$ in the voltage feedback loop. The resulting closed loop poles and zeros for six operating points, representing the extremes of maximum motoring torque, maximum regenerative braking torque, high-speed, low speed operation, and dynamic braking are shown. Only the dominant pole and zero locations are tabulated. The gain of the compensator $K_v$ was again varied by means of a root-locus program. Although the gain for optimum location of the poles does not change with speed, the optimum gain setting changes for motoring, regenerative braking, and dynamic braking.

Examination of Table II indicates that even with optimum compensator gains the transient response during braking is not satisfactory. In general, fast response to

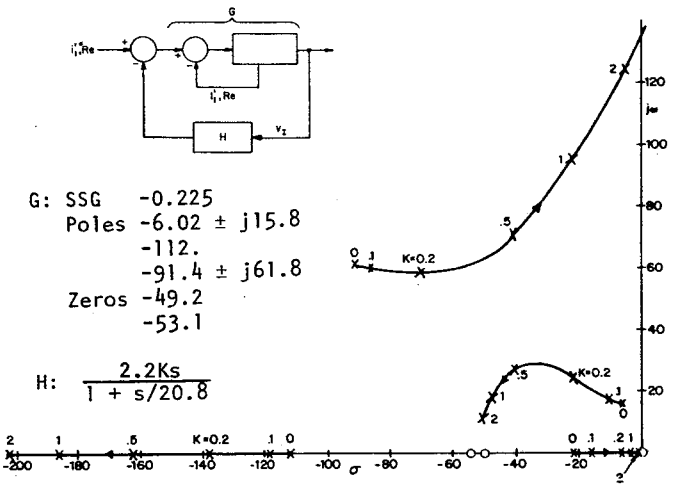


Fig. 19. Voltage derivative feedback, operating point: 60 mi/h $T = -820$ ft·lb.

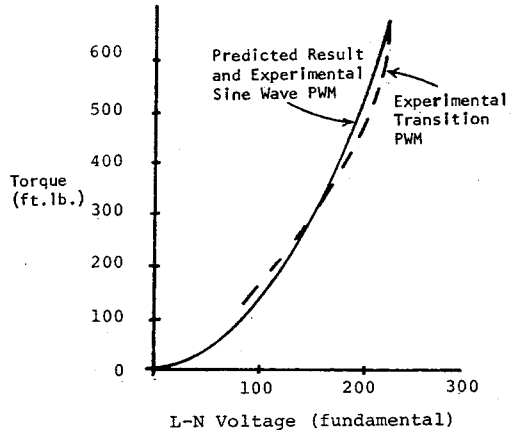


Fig. 20. Comparison of predicted and measured torque.

line transients is desirable during regenerative braking to minimize torque disturbances. Also, an additional feedback loop is desirable in order to provide additional damping during dynamic braking. In order to improve braking performance, an additional feedback from the dc inverter voltage to the $i_{1,Re}'$ summing point is used.

Fig. 18 shows a block diagram of the final system. The compensators $C_f$ and $C_v$ which were finally selected are explicitly shown. Because of the braking resistors used during dynamic brake, the control study indicates that the gain of the voltage channel must be changed during this mode. The cross-coupling multiplier between the frequency and voltage channels can be noted. The additional damping signal for braking is shown entering the upper summing point.

In Fig. 19 the curves are plotted for a typical root locus of the closed system with the voltage feedback closed. The case selected is for dynamic braking at 60 mi/h. The dominant open-loop poles and zeros are shown in the inset block. It was found that the addition of voltage feedback allows for an increase of gain in the primary slip control channel without instability in dynamic braking and significantly improves the closed-loop bandwidth.

## EXPERIMENTAL RESULTS

The induction motor control strategy which has been outlined was implemented and tested on both a detailed analog computer simulation and an actual system. The results indicate that the system performs as predicted except for harmonic current effects caused by the inverter voltage waveform. In the practical system, three types of inverter waveform are used: a sine wave shaped pulse-width modulation, a special transition mode of PWM, and square wave operation. The latter two methods contain a considerable component of harmonics phase synchronized to the fundamental current.

The method of calculating the in-phase component of motor current consists of adding a sine wave proportional to the motor voltage to $-IR$ (stator resistive voltage drop) and then using the zero crossings of $(V - IR)$ to throw a switch between $+I$ and $-I$. The net result is a switching phase detector which responds to the fundamental and all harmonics with a gain reduction factor for higher harmonics that are in phase with the fundamental. Nonsynchronized harmonics, such as in sine wave shaped PWM, produce no average output.

The results of measurements on the hardware show that the $i_{1,Re}'$ signal responds accurately for sine wave shaped PWM for a nonsynchronized chopping frequency. Synchronization causes less than a 5 percent error in the $i_{1,Re}'$ calculation. However, for both square wave operation and transition mode PWM, significant errors are observed due to the phase synchronized harmonics. Filtering of the current feedback into the $i_{1,Re}'$ circuit gives the correct result except in transition PWM. The measured torque plotted in Fig. 20 indicates that the motor actually produces some average torque due to the 5th and 7th harmonics in the transition PWM mode. Although an analysis of the motor using the normal equivalent circuit and including deep bar rotor resistance effects does not predict this effect, it can, if necessary, be corrected by inserting an offset in the torque command signal during these two modes of operation.

## CONCLUSION

Advances in solid-state power conversion devices have provided new opportunities in the application of ac induction motors to variable speed drive applications formerly achievable only with dc motors. This paper has described an analytical and experimental process for the evaluation of several methods of controlling torque in an inverter-induction motor propulsion drive and has pointed out several problems which have been overcome in the system design.

Of the systems discussed, the control using a modified value of real current has realized the desired steady-state and transient performance over the range of speed and torque required for a transit application. With suitable modification, a torque controller can be used to perform numerous tasks. Hence, it is expected that this control

method should find acceptance in other speed control applications.

## NOMENCLATURE

| | |
|---|---|
| $\sim$ | Phasor. |
| $\Delta$ | Small change from steady-state. |
| * | Commanded quantity as in $f_{sl}$*. |
| SSG | Steady-state gain (dc gain). |
| TF | Transfer function. |
| $f_b$ | Base frequency (hertz). |
| $f_e$ | Stator (inverter) frequency (hertz). |
| $f_r$ | Equivalent rotor speed (hertz). |
| $f_{sl}$ | Slip frequency (hertz). |
| $i_1$ | Phase current amplitude (root mean square amperes). |
| $i_{1,\mathrm{Rc}}'$ | Real component of phase current with respect to terminal phase voltage (root mean square amperes). |
| $i_{1,\mathrm{Re}}'$ | Real component of phase current with respect to phase voltage inside stator $IR$ drop (root mean square amperes). |
| $T$ | Shaft torque or average electromagnetic torque (foot pound). |
| $v_1$ | Terminal phase voltage (root mean square volts). |
| $v_1'$ | Phase voltage inside stator $IR$ drop (root mean square volts). |
| $v_b$ | Base phase voltage (root mean square volts). |
| $V_1$ | Phase voltage divided by per unit frequency. [See (1)] (root mean square volts). |

## REFERENCES

[1] R. H. Nelson, T. A. Lipo, and P. C. Krause, "Stability analysis of a symmetrical induction machine," *IEEE Trans. Power App. Syst.*, vol. PAS-88, pp. 1710–1717, Nov. 1969.

[2] T. A. Lipo and P. C. Krause, "Stability analysis of a rectifier-inverter induction motor drive," *IEEE Trans. Power App. Syst.*, vol. PAS-88, pp. 55–66, Jan. 1969.

[3] T. A. Lipo and A. B. Plunkett, "A novel approach to induction motor transfer functions," *IEEE Conf. Rec., of IAS 1973 8th Annu. Meet. of the IEEE Ind. Appl. Soc.*, pp. 441–449, Oct. 8–11.

**A. B. Plunkett** (S'66–M'70) was born in Portsmouth, Ohio, on March 7, 1941. He received the B.S.E.E. degree from Texas Western College, El Paso, in 1965, and the M.S.E.E. and Ph.D. degrees from the University of Texas, Austin, in 1967 and 1970, respectively.

Since 1970 he has been employed by the Transportation Equipment Products De-Department, General Electric Company, Erie, Pa., where he has been engaged in the development of induction motor drive systems.

Dr. Plunkett is a member of Eta Kappa Nu, Tau Beta Pi, and Sigma Xi.

**Thomas A. Lipo** (M'64–SM'72) was born in Milwaukee, Wis., on February 1, 1938. He received the B.E.E. degree with honors and the M.S.E.E. degree from Marquette University, Milwaukee, in 1962 and 1964, respectively, and the Ph.D. degree in electrical engineering from the University of Wisconsin, Madison, in 1968.

From 1959 to 1964, he completed both the Cooperative Training Course and the Graduate Training Course at the Allis-Chalmers Manufacturing Company, Milwaukee, Wis. During 1968–1969, he was a S.R.C. Postdoctoral Fellow at the University of Manchester Institute of Science and Technology, Manchester, England. Since 1969, he has been an Electrical Engineer in the Physics and Electrical Engineering Laboratory, Research and Development Center, of the General Electric Company, Schenectady, N.Y. During the academic year 1973–1974, he was a visiting Associate Professor at Purdue University, West Lafayette, Ind. At General Electric, he has been engaged in the simulation, analysis, and control of static converter systems for a variety of applications including linear motors, static exciters, ball mills, turbine-generator rotor balancing, and traction drives for rail and off-highway vehicles.

Dr. Lipo is a member of Eta Kappa Nu, Pi Mu Epsilon, Tau Beta Pi, and Sigma Xi.